Electronic Supplementary Material (ESI) for Physical Chemistry Chemical Physics.

Electronic Supplementary Information

Electrochemical evaluation of the de-/re-activation of oxygen evolving IrO_x

Georgios Papakonstantinou,[a] Ioannis Spanos,[b] An Phuc Dam,[a] Robert Schlögl,[b,c] Kai Sundmacher[a,d]

[a] *Max Planck Institute for Dynamics of Complex Technical Systems, Process Systems Engineering, Sandtorstr.1, D-39106 Magdeburg, Germany*
[b] *Max Planck Institute for Chemical Energy Conversion, Department of Heterogeneous Reactions, Stiftstr. 34-36, D-45470, Mülheim an der Ruhr, Germany*
[c] *Fritz Haber Institute of the Max Planck Society, Department of Inorganic Chemistry, Faradayweg 4, D-14195 Berlin, Germany*
[d] *Otto-von-Guericke University Magdeburg, Process Systems Engineering, Universitätsplatz 2, D-39106 Magdeburg, Germany*

1. Charge assessment and influences of substrate and purging gas with the RDE setup

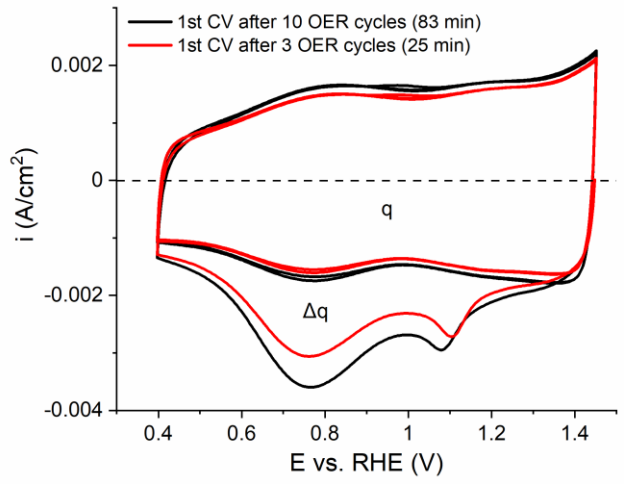

Figure S1: The CVs displayed in Fig. 2b (after 10 OER cycles, black, and after 3 OER cycles, red). The as measured current densities are displayed to show the small differences in the loading between the two catalyst layers (nominal IrO_x loading 50 μg/cm^2). q is the charge of the final (3rd in this case) cathodic sweep, while Δq (= $q_{c,i} - q_{c,f}$) is the difference between the initial and the final cathodic sweeps. Some residual cathodic charge in the 2nd cathodic sweep is also accounted for in Δq integrations (see also Fig. S2 below).

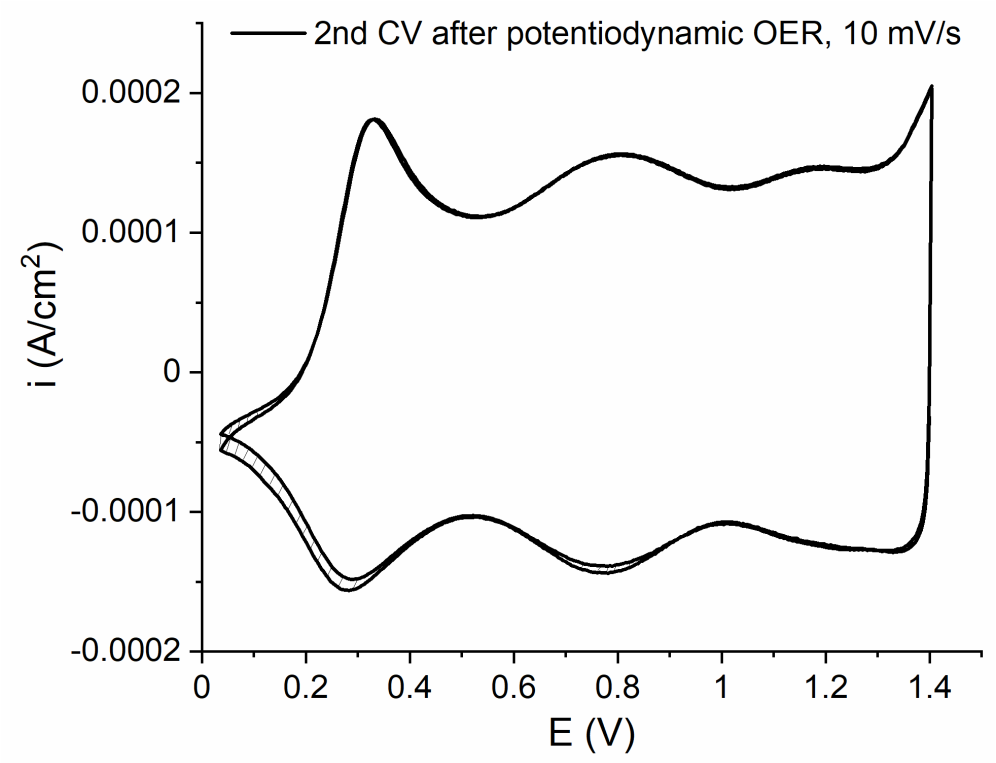

Figure S2: Staircase CV with 10 mV/s (1.4-0.04 V, 2 cycles) acquired after 3x OER cycles (Fig. 2a) and a CV with 50 mV/s and LPL = 0.4 V (3 cycles, Figs. 2b and S1). The shaded highlighted regions show the residual charge, which was previously grown during OER and not passed in the preceding CV. There is some residual charge in the potential regions 0.04-0.4 V and 0.6-0.9 V, due to incomplete reductions in the preceding CV cycles. These additional cathodic charge contributions are accounted in the charge integrations as part of the OER induced excessive cathodic charge.

CVs with LPL = 0.04 V are always measured after at least three CV cycles with LPL = 0.4 V (Fig. S1), when aiming in full regeneration of the OER activity, in order to allow for sufficient time with N_2 purging for the effective removal of O_2 from the solution, and suppress Au/ORR contributions below 0.4 V (see Fig. S5 further below) that may skew charge assessment.

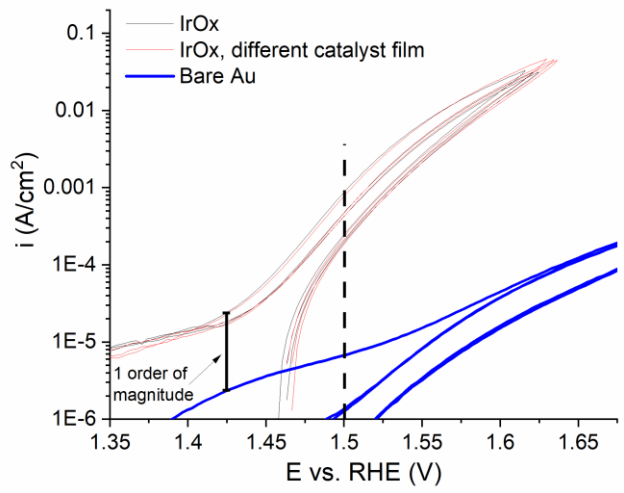

Figure S3: Three potentiodynamic OER cycles (1.3-1.8 V, 2 mV/s) with two different catalyst layers of same nominal Ir loading (black and red lines). OER sweeps with bare Au (blue lines) are embedded to show that Au influence on OER activity is negligible (more than one order of magnitude lower current, especially at 1.5 V, RHE, chosen as a representative metric of de-activation/re-generation). Au surface oxide is mainly grown during the 1st anodic OER sweep, in the 1.4-1.55 V potential range.

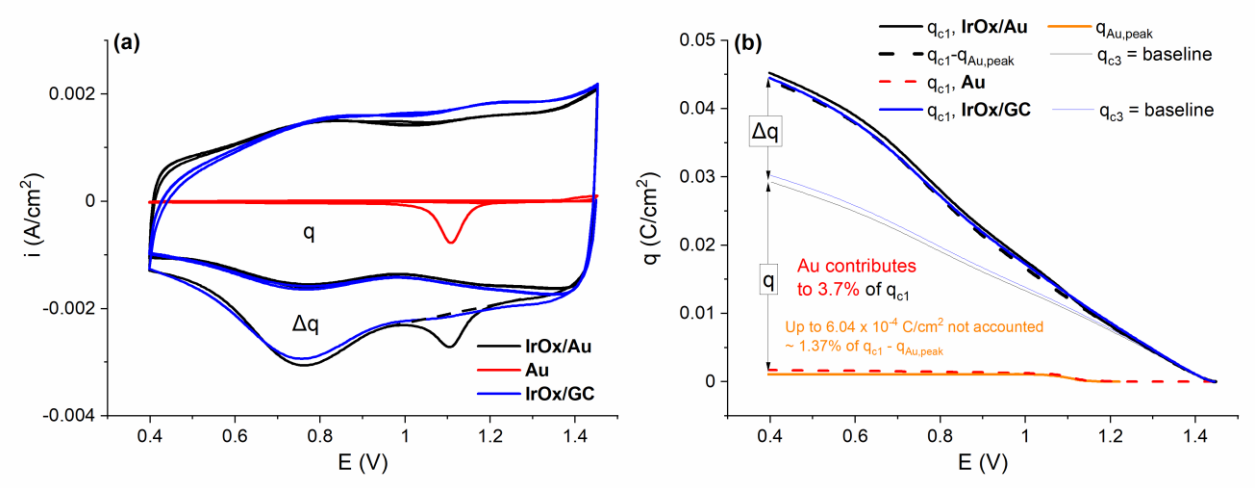

Figure S4: (a) Staircase CVs (50 mV/s) after potentiodynamic OER with IrOx on Au (black line) and glassy carbon, GC (blue line), substrates, as well as with bare Au (red line). Au oxide reduction at ca. 1.1 V is subtracted with the straight black dashed line as background to provide $\Delta q = q_{c,1} - q_{Au} - q_{c3}$, free from Au contributions, as a fair approximation. **(b)** The respective cathodic charge integrations show that the reduction of Au oxide contributes to 3.7 % of q_{c1}. Rest of Au contributions are ≤ 1.37 % of q_{c1} - q_{Au} and therefore can be omitted.

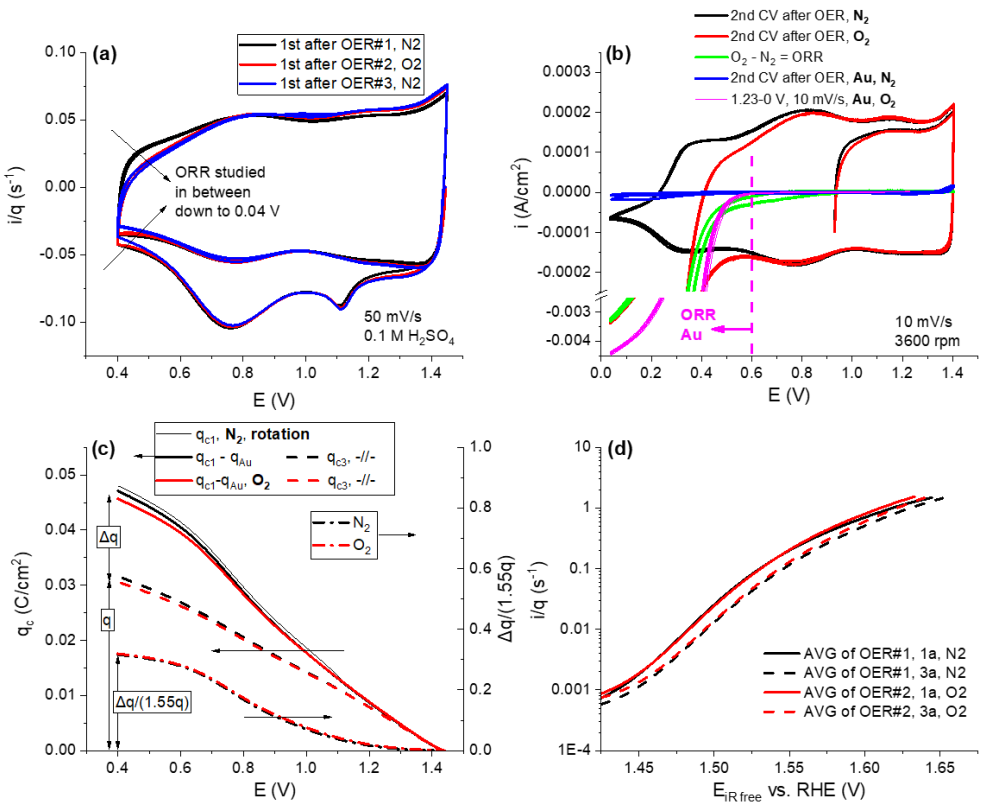

Figure S5: (a) Staircase CVs (50 mV/s, sampling parameter α = 1, potential step height 4 mV) measured after OER sweeps with N_2 (black and blue) and O_2 (red) purging with IrOx/Au. Slight ORR contributions may be discerned below 0.5 V. **(b)** Staircase CVs (10 mV/s) with N_2 (black) and O_2 (red) purging. ORR onset commences at ca. 0.6 V, 100 mV higher potential than in (a) due to the lower sweep rate. Their subtraction (green) almost overlaps with the ORR on bare Au (magenta), indicating that ORR activity comes from the Au substrate. A second CV (blue) after performing OER sweeps on Au and three CV cycles down to 0.4 V with 50 mV/s is added to show the effective O_2 removal by N_2 purging. **(c)** Charge and $\Delta q/(1.55q)$ evaluations on IrOx/Au with N_2 (black) and O_2 (red) purging. The empirical multiplication factor 1.55 on q is used to account for the suppression of the double-layer non-faradic contributions and those of fast processes in the staircase CVs with sparse current sampling (50 mV/s, 4 mV step height, sampling parameter α = 1) and it is explained in Fig. S17 further below. The gas atmosphere does not influence the charges integrated down to 0.4 V. **(d)** Average of base CV charge normalized anodic OER sweeps (2 mV/s,

post-test iR correction) from three different IrOx catalyst films of same nominal IrOx loading with N_2 (black) and O_2 (red) purging. First (solid) and third (dashed lines) anodic sweeps are displayed to show the deactivation without overcrowding the figure. Noteworthy that the presence of O_2 in the electrolyte is not affecting OER activity, suggesting that the O_2 evolution step is not rate limiting, and that the OER kinetics do not follow any dependence on the partial pressure of O_2 and its influence on the Nernst potential, at least with the hydrous IrOx catalyst.

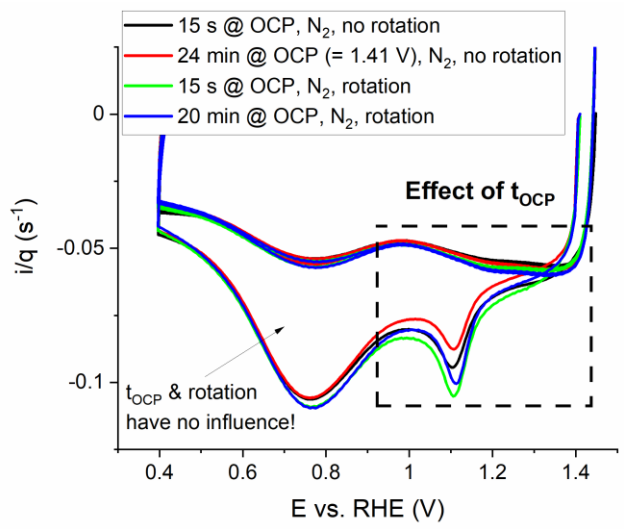

Figure S6: Influence of time at open circuit conditions on the cathodic sweeps down to 0.4 V with 50 mV/s. Up to 20 minutes with rotation (blue) or 24 minutes without rotation (red), in comparison to short times (≈15 s) at OCP (black and green) after interrupting OER at 1.45 V. t_{OCP} influences the OCP value (40 mV decay in 24 minutes, not recorded to avoid forced discharge), and the charge at $E > 1$ V (dashed rectangle), whereas the low potential charge is not influenced for t_{OCP} up to 20-24 min under N_2 purging with (green and blue) or without (black and red) rotation. Thus, ORR contributions are safely excluded in q and Δq assessments. The difference in the intensity of the Au reduction peak is due to differences in the IrOx loading, hence the charge normalization on the current density.

2. Influences of ionomer and electrolyte on the eQCM responses

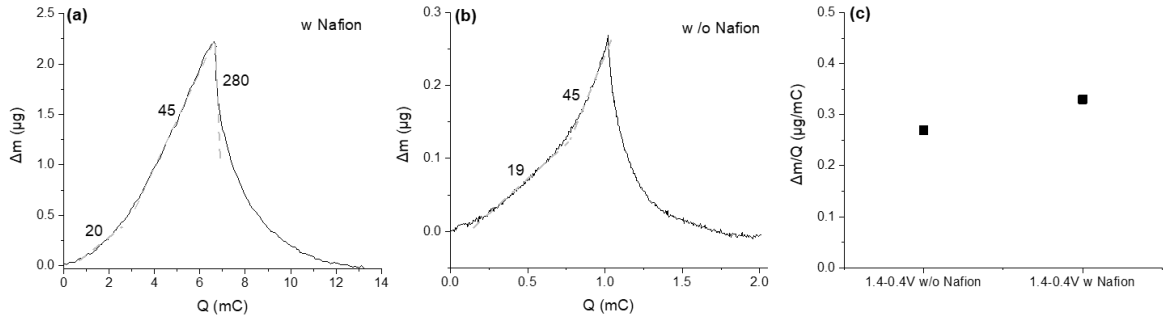

Figure S7: eQCM mass variations during CVs (0.4-1.4 V) with **(a)** and without **(b)** Nafion ionomer film atop the catalyst layer against the CV charge (absolute integration). The mass variation is one order of magnitude lower in the absence of ionomer due to the inherent instability of the catalyst film during the preceding potentiodynamic OER. Nevertheless, the mass-to-charge ratios agree in presence and absence of ionomer atop the catalyst film. **(c)** The integral mass-to-charge ratios of a full cathodic sweep with and without Nafion film agree fairly well ($\Delta m/Q \approx 0.3 \pm 0.03$ µg/mC).

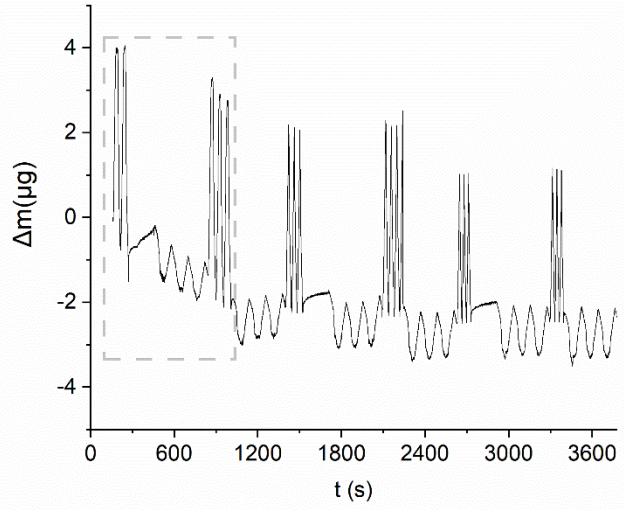

Figure S8: Mass variations during sequential CV-OER-CV measurements over time. LPLcv = 0.04 and 0.4 V. The mass decrease in the first 10-15 min (grey dashed rectangle) may be attributed

to changes in the viscoelastic properties of the catalyst/ionomer film, due to initial hydration (wetting), without excluding the influence of Ir dissolution and detachment of aggregates, the latter usually intensified during the first three potentiodynamic OER cycles (e.g. see charge evolution with time during potentiodynamic OER/CV measurements with RDE in Fig. S13).

In a recent study with Au coated quartz crystals, binder free IrOx and higher loadings than those in our study,[1] it was proposed that the elastic character of the film dominates, and the frequency changes were directly related to intrinsic film mass changes. The presence of Nafion ionomer atop the catalyst film did not show significant variations with respect to the frequency responses in the absence of ionomer (Fig. S7), apart from an inherent instability of the binderless catalyst film, attributed to the detachment of catalyst aggregates during OER, optically observed after test. The influence of changes in viscoelasticity, e.g. due to hydration and swelling of the ionomer, is probable in the first measurements after immersion of the eQCM probe in the electrolyte (Fig. S8, highlighted with a dashed grey rectangle). Thereafter, the frequency changes are essentially reversible.

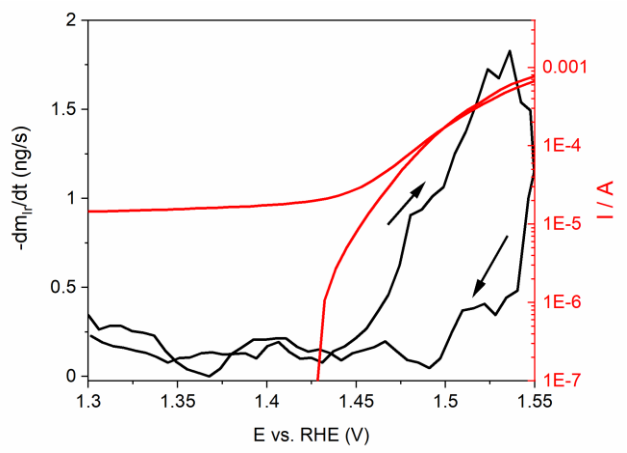

Figure S9: Current (right y-axis, red) and Ir dissolution rate (left y-axis, black) during a full OER cycle. Dissolved Ir was followed on-line with ICP-OES. Dissolution commences with the OER onset at ca. 1.45 V. The integrated amount of Ir dissolved in a full cycle is 27.3 ng.

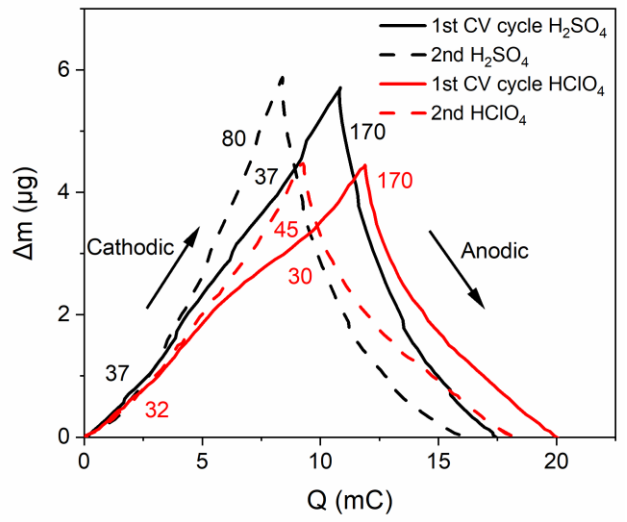

Figure S10: Mass profiles against the CV charge (absolute integration) in the course of two consecutive CVs (1.4-0.4 V, RHE, 50 mV/s) subsequent to OER cycles (first, solid and second cycle, dashed lines) in 0.1 M H_2SO_4 (black) and 0.1 M $HClO_4$ (red).

3. Influence of the cathodic potential and charge on the regeneration of the OER activity

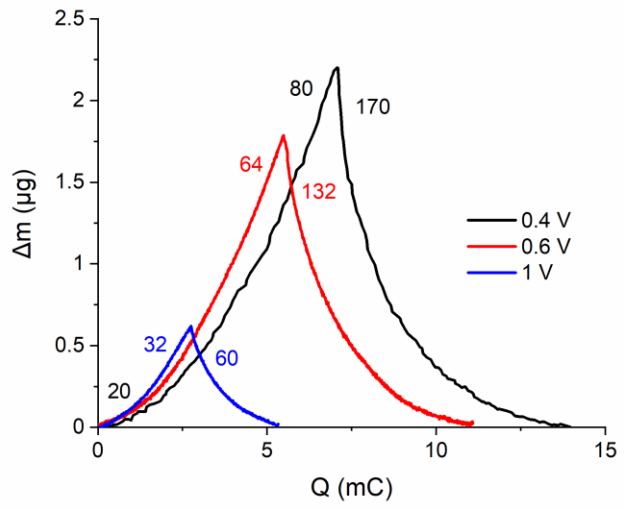

Figure S11: Mass changes vs. the CV charge (absolute integration) during the second CV cycles (5 mV/s, eQCM flow cell), after potentiodynamic OER without current interruption, with different LPL (legend in the figure). The first CV cycles are displayed in Fig. 4b.

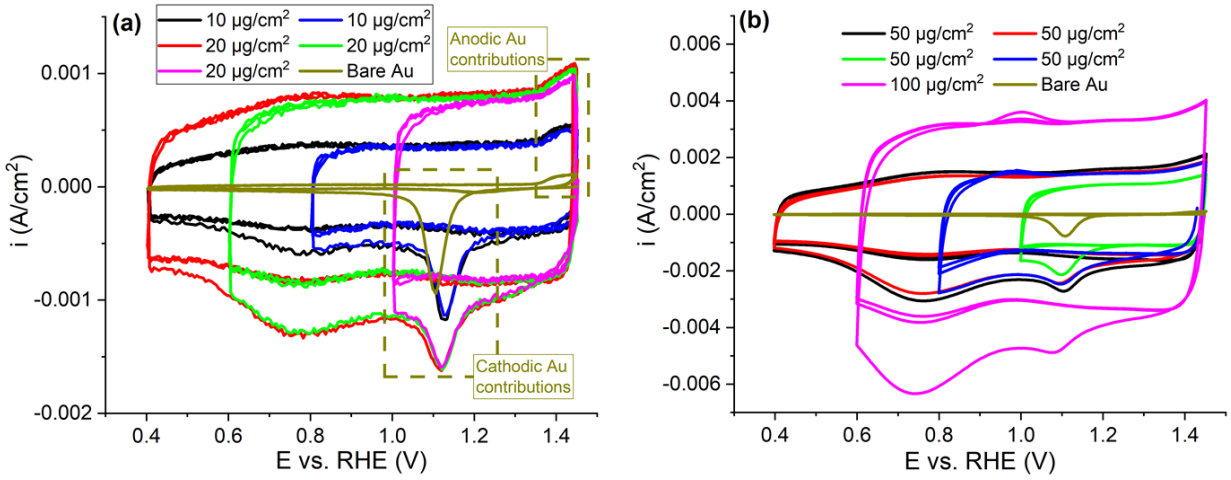

Figure S12: (a) Linear ramp CVs (50 mV/s) after potentiodynamic OER/15 s OCP with different LPL and two different IrOx loadings (10 and 20 μg IrOx/cm^2). Reference CV with Au in dark yellow (dark yellow dashed rectangles declare the regions that Au features become significant). Contributions from Au oxide reduction at ca. 1.1 V increase with decreasing IrOx loading. Rest of

Au contributions can be neglected (e.g. Fig. S4). **(b)** Staircase CVs (50 mV/s, sampling parameter $\alpha = 1$, step height 4 mV) with different LPL on different catalyst films with 50 μg IrOx/cm^2 nominal loading (100 μg IrOx/cm^2 also included, magenta). Δq is not entirely passed in one CV cycle with 50 mV/s and LPL ≥ 0.4 V. The amount of Δq in the subsequent sweeps increases with increasing LPL. An anodic peak at ca. 1 V emerges, which decays with the number of cycles. It becomes maximal when LPL = 0.6 V. Au reference CV also included (dark yellow).

Although the anodic peak at ca. 1 V is barely discernible during linear ramp CVs (Figs. 4a and S12a), it always appears after the first cathodic sweep subsequent to an OER measurement in staircase CVs (Figs. S12b and S14 below), in which the double-layer non-faradic contributions are suppressed when the sampling parameter $\alpha = 1$ (defined as $\alpha = 1 - \tau'/\tau$, τ the potential step width that equals the potential step height over the sweep rate, $\Delta E/\upsilon$ = 4 mV/50 mV/s = 0.08 s in Fig. S12b), and τ' the sampling interval defined by parameter α).[2] The peak intensity decreases with the number of cycles until it disappears after few CV cycles, and it scales with catalyst loading (Figs. S12b and S14 below), i.e. it is more intensive for thicker catalyst films. The peak potential is slightly higher (by ca. 50 mV) than that of a reversible pair of peaks observed in CVs of glassy carbon in Ir containing solutions, which were obtained from the chemical dissolution of Ir-based perovskites.[3] This pair of peaks was attributed to the precipitation potential of UV-vis active (at ca. 520 nm) Ir dissolved species. Noteworthy that the anodic peak is barely discernible in the CVs acquired with the flow cell (not shown), due to the CV settings that approach linear scan conditions (sampling time $\tau' = \tau$ = 0.02 s vs. 0.08 s in the staircase CVs in Fig. S12b). When more than 50% of the excessive cathodic charge has been passed, i.e. at potentials lower than the main cathodic peak, the anodic peak is more intense and disappears faster than when less than 50% of the charge has been passed, i.e. at potentials more positive than the main cathodic peak. Based on that, it might

be speculated that its presence is linked with the formation of partially reduced species, which subsequently are oxidized, exposing redox behavior, provided that sufficient amount of H^+/H_2O has been intercalated in the previously oxidized anionic framework of the IrOx structure. Such behavior might arise from species with (hydro-)peroxo-character, able to be oxidized at potentials higher than the equilibrium potential of H_2O_2/O_2, releasing O_2.[4] Nevertheless, as the charge involved is very low, it is omitted in the charge integrations.

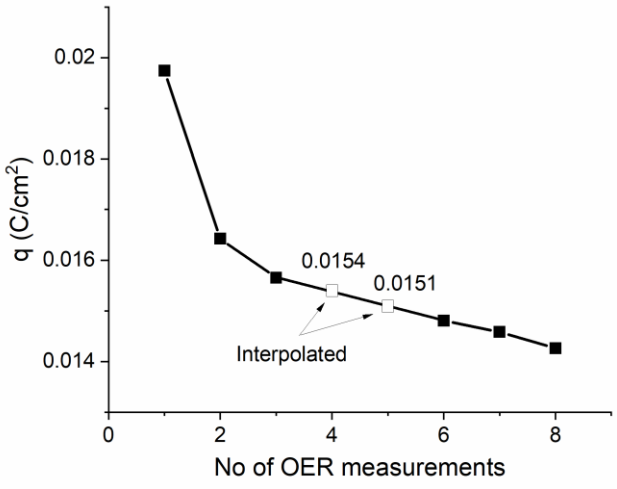

Figure S13: Example of the CV (0.4-1.45 V, 50 mV/s) charge profile vs. the number of potentiodynamic OER/CV sequencies, measured before each sequence, and its interpolation (hollow symbols) when linear ramp CVs with LPL > 0.4 V were pursued (Fig. 1a). Data correspond to one of the two experiments presented in Fig. 4a. Au tip, 20 μg IrOx/cm^2 nominal. *q* loss is mostly due to detachment (strong initial decay after the 1st potentiodynamic OER) and relates to the quality of the catalyst/ionomer self-assembly of the composite film. In some experiments, *q* was stable, as for example in the measurements involving 10 potentiodynamic OER cycles in Fig. 2a.

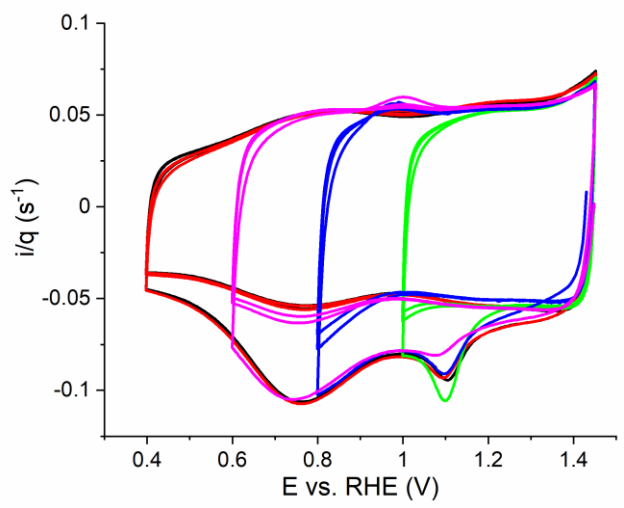

Figure S14: Staircase CVs (50 mV/s, 3 cycles, sampling parameter α = 1) with different LPL (0.4 – 1 V) performed after potentiodynamic OER measurements with different catalyst films (as measured current densities in Fig. S12b)**.** The charge normalization results in highly overlapping CVs, despite the differences in the IrOx loading (50 µg IrOx/cm^2 nominal in all CVs, except in magenta, 100 µg IrOx/cm^2).

4. Influence of the type of CV, staircase or linear ramp, on charge

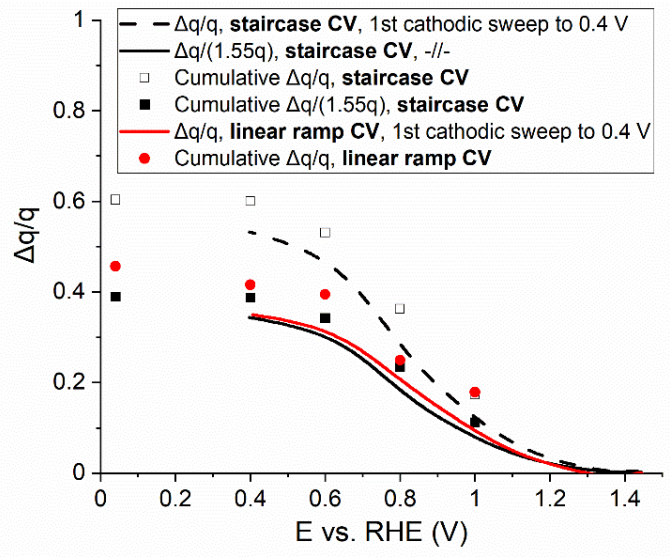

Figure S15: Fractional cumulative excessive cathodic charge of all CV cycles measured after OER, over the base CV charge ($\Delta q/q$) (symbols), and the charge fraction profiles of the first cathodic sweeps down to 0.4 V (lines) vs. the applied LPL_{CV}. Au oxide contributions are subtracted, as illustrated in Figs. 4a and S4. The charge fractions assessed by linear ramp (red) and staircase (black) CVs are displayed. The staircase CVs were measured with sampling parameter $\alpha = 1$ (data from Fig. S12b). The as measured charge fraction profiles with staircase CVs are shown with hollow symbols and dashed line. Upon applying the empirically assessed correction factor $f = 1.55$ (see Fig. S17 further below), to correct the underestimated base CV charge of the staircase CVs, $f \cdot q$, the charge fractions converge (black filled symbols, solid line) with the respective values assessed by linear ramp CVs (red).

Staircase CVs with sparse current sampling (0.08 s after stepping the potential) underestimate the double-layer charging currents, as well as that related to fast processes.[2,5] Meanwhile, the evaluation of Δq is not influenced significantly by the type of the CV measurement. This is explicitly

shown in Fig. S16 below, in which staircase CVs with 50 and 5 mV/s are presented, both measured after three potentiodynamic OER cycles, interrupted at 1.45 V cathodic and few seconds at OCP. The sweep rate in staircase CVs was varied through change in step width, τ, by keeping the same integral number of potential steps and hence the same step height, ΔE, while the sampling parameter α was set to 1 (the current was sampled at the end of each potential step, resulting in 0.8 s sampling the current after stepping the potential with 5 mV/s, vs. 0.08 s sampling with 50 mV/s).[2,6] Although the overall current response normalized to the sweep rate at 5 mV/s, especially that of the subsequent sweeps that are mostly associated with double-layer like charging currents (see also Fig. S17b below), is significantly lower than that expected only by the variation in the sweep rate (Fig. S16a), Δq (= $q_{c1} - q_{c3}$) is not influenced by the sweep rate (see in Fig. S16b for the charge integrals).

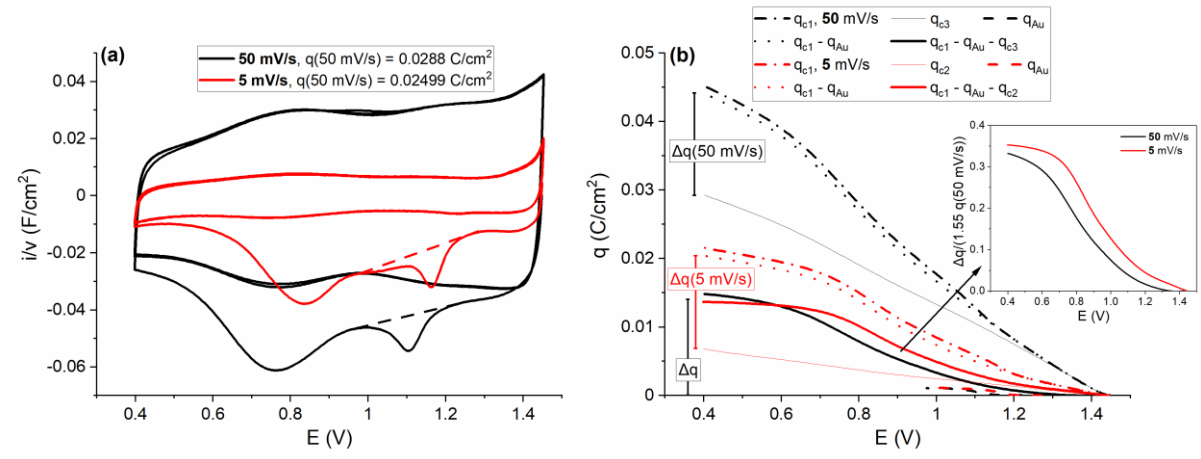

Figure S16: (a) Staircase CVs (α = 1, ΔE = 4 mV), measured after interrupting 3 OER cycles at 1.45 V cathodic, with 50 mV/s (black) and 5 mV/s (red), with the current density normalized to the sweep rate. The dashed lines display the background used for subtracting the charge contributions

from the reduction of the Au oxide formed during the preceding OER sweeps. **(b)** Respective integrations (colors as in left), Au oxide subtractions (dashed lines) and Δq evaluation (thick solid lines). $\Delta q/(1.55q(50\ \text{mV/s}))$ profile vs. potential in the inset shows the shift to higher E with decreasing sweep rate, but also the enhancement of reductions with decreasing sweep rate. Note that all anodic sweeps, and cathodic sweeps except the first after OER, highly overlap, indicating that the OER formed charge is consumed in the first cathodic sweep down to 0.4 V when slow sweeping is applied. The empirical factor 1.55, used only to correct the charge of the base voltammograms in staircase CVs with 50 mV/s and sparse sampling ($\alpha = 1$, $\tau' = \tau = 0.08$ s), is assessed by comparing the staircase CVs with linear ramp CVs performed on the same catalyst film (see below in Fig. S17a).

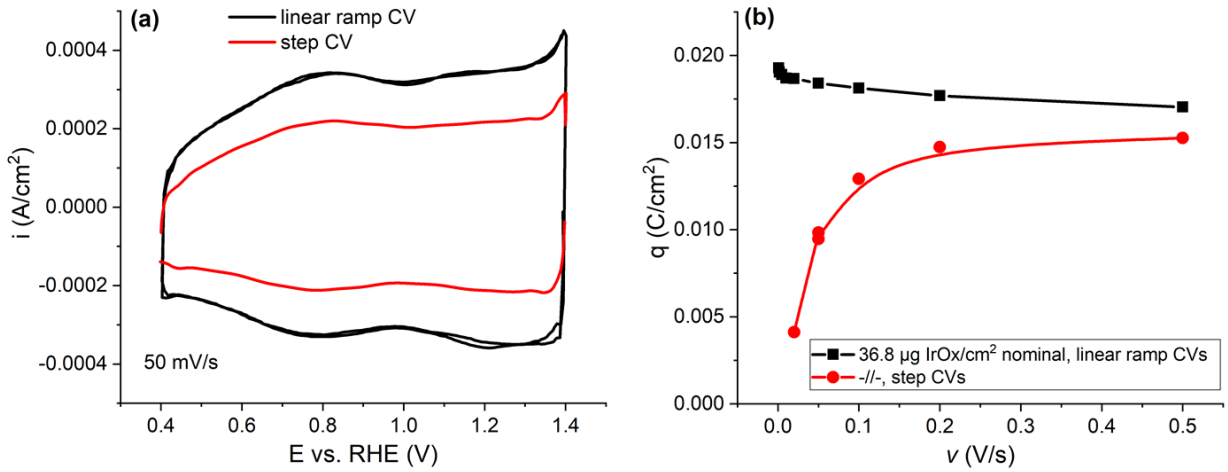

Figure S17: (a) Base voltammograms performed consecutively on the same catalyst film (Fig. 5a, 20 µg IrOx/cm^2 nominal loading) undergone the potentiodynamic de-/re-activation protocol, with two different potentiostats performing staircase CVs (red), with sampling parameter $\alpha = 1$ and the same settings as those used in the measurements in Figs. 2b, 5b, 6, S12 and S14-17, and linear ramp CVs (black). The charge ratio between the two measurements is $f = q(\text{linear ramp CV})/q(\text{staircase CV}) = 1.55$, which is used in correcting the base CV charge in staircase voltammetries with

sampling parameter α = 1, 50 mV/s sweep rate and 4 mV step height, on the assumption that f depends only on the measuring settings, and catalyst film properties do not affect it. **(b)** The base CV charge of linear ramp (black) and staircase (red) voltammetries against the sweep rate for two different catalyst films (nominal loading 36.8 μg IrOx/cm^2). With increasing sweep rate, the charges assessed with the two different types of CVs converge, whereas staircase CVs with sparse sampling (α = 1, ΔE = 4 mV) underestimate the charge at sweep rates ≤ 200 mV/s. The step height was kept constant (4 mV), so that the step width and current sampling time increase with decreasing sweep rate for constant sampling parameter α = 1.

5. Charge normalized OER activity decay and regeneration under potentiodynamic OER conditions; influence of time

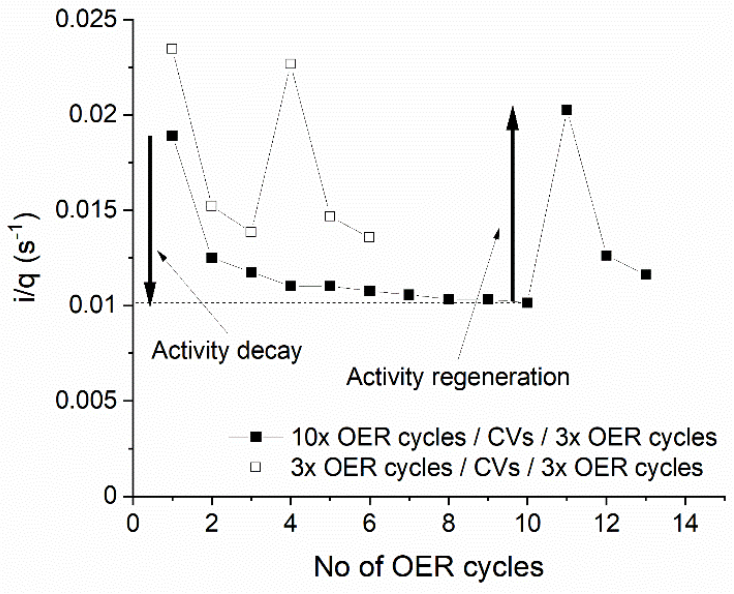

Figure S18: Base CV (0.4-1.4 V, 50 mV/s) charge normalized OER activity at anodic 1.5 V, RHE, post-test iR corrected, vs. the number of OER cycles, in the context of potentiodynamic OER (2 mV/s). The activity decay and the respective regeneration are shown in the figure with arrows. When dividing with the initial charge normalized activity, the fractional activity loss and regeneration are obtained. First three (hollow symbols) and ten OER cycles (filled symbols) are plotted in Fig. 6. The difference in the charge integrals between the first and the second anodic OER sweeps is more than one order of magnitude higher than Δq assessed by the regenerative CVs, and therefore cannot be ascribed only to adsorption/oxidation/dissolution processes, but majorly to variations in OER activity.

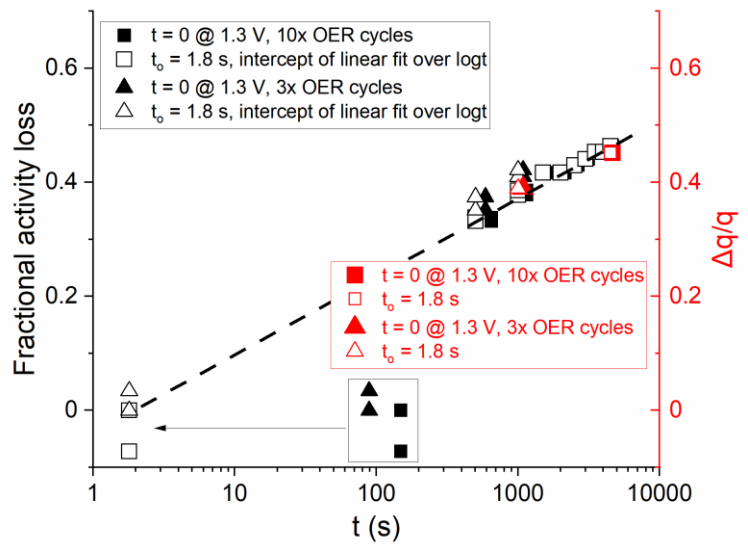

Figure S19: Fractional activity loss (black symbols, left-y axis) at 1.5 V, RHE, assessed on the anodic portion of the potentiodynamic OER cycles (2 mV/s, 1.3-1.8 V, data from Figs. 2a and S18) against time in logarithmic scale. The fractional charge grown during potentiodynamic OER, measured upon sweeping to 0.4 and 0.04 V (e.g. Figs. 2b and S2) after interrupting OER at 1.45 V cathodic, is also embedded (red symbols, right-y axis). Note that the base CV charge in the denominator of the fractional charge is multiplied by the empirical factor 1.55, in order to account for the charge suppression in the base CVs with sampling parameter α = 1 (Fig. S17). Solid symbols are plotted against t = 0 s the time at which the OER sweeps are initiated (at 1.3 V, RHE). The respective open symbols are shifted to the intercept of y-axis (fractional activity loss = 0), t_o = 1.8 s, of the linear fit of the fractional activity loss vs. log$t$ (dashed line) that includes data from the second OER cycle and above (see discussion below).

When considering as t = 0 at E = 1.3 V, RHE, i.e. when starting the OER sweeps, the apparently linear fractional activity loss on log$t$ includes all OER cycles from the second and above. The linear regression vs. log$t$ provides t_o = 1.8 s intercept, suggesting that the deviation of the first measuring point from the linearity vs. log$t$ comes from the arbitrary selection of t = 0 s, while its influence on the fitting can be safely neglected at times longer than one order of magnitude. The intercept t_o =

1.8 s (respective open symbols in Fig. S19) is almost equal to the current sampling time (potential step height over the sweep rate, 3.2 mV / 2 mV/s = 1.6 s, with sampling parameter $\alpha = 1$), which is ca. ten times the estimated cell time constant, $\tau_{cell} = R \cdot C_{dl} \approx 0.15$ s,[7] hence resulting in almost full suppression of non-faradic charging currents.[7] The consistency between the intercept of the fractional activity loss vs. log*t* and the current sampling after stepping the potential to 1.5 V, RHE, suggests that the log*t* dependent activity decay starts already at short times. Therefore, in the inset of Fig. 6 the current sampling time after reaching 1.5 V, RHE, is used ($t_o = 1.6$ s), which is included in the respective linear fits presented in the inset of Fig. 6 ($R^2 \geq 0.997$). Note that only the data from the first OER sequences (10x and 3x OER cycles) are displayed in the inset in Fig. 6 for better visibility.

6. De-/Re-activation under potentiostatic OER conditions

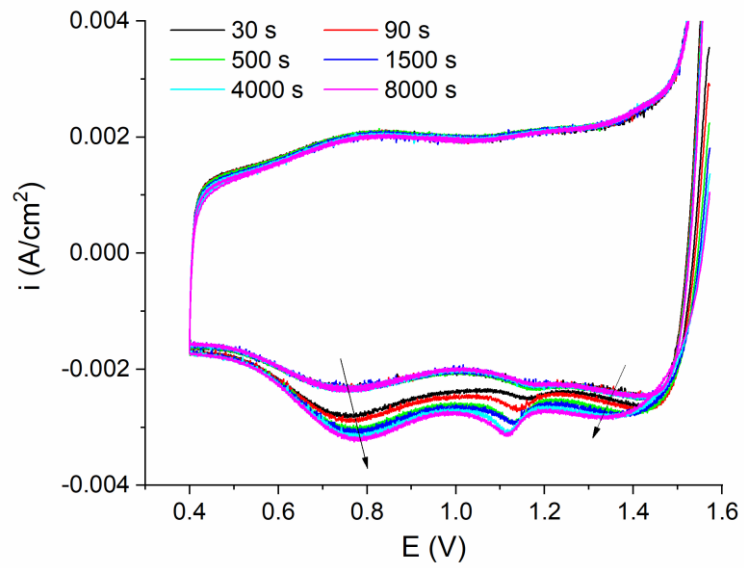

Figure S20: Staircase CVs after different potentiostatic time intervals (see legend in the figure) at *iR* compensated 1.575 V, RHE, performed with the RDE half-cell. These staircase CVs were acquired with 50 mV/s sweep rate, 0.5 mV step height, and sampling parameter α = 0.3. With these measuring settings linear sweep voltammetry conditions are approached for reversible and quasi-reversible processes.[2,5] Hence, the correction factor *f* (= 1.55) was not multiplied on the base CV charge in this case. The charge fraction grown in three OER cycles (green curve in Fig. 7) agrees with the respective values deduced by linear ramp CVs (e.g. Figs. 4a and 5) and with those assessed by staircase CVs with sampling parameter α = 1, after applying the base CV charge correction factor *f* = 1.55 (Figs. 6, S15 and S17).

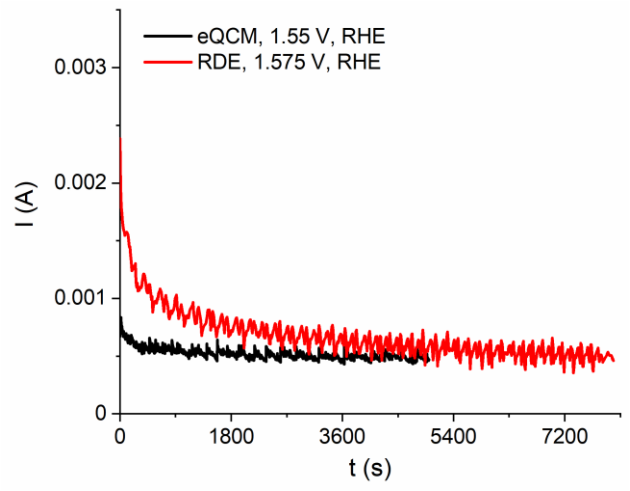

Figure S21: (a) Current profiles over time of two representative stationary operation interims. The influence of bubbles in the current profiles is discerned, which creates chainsaw patterns, being more intensive in the RDE configuration, presumably due to the horizontal electrode orientation despite the rotation. The eQCM electrode with vertical orientation takes the advantage of buoyancy in the removal of bubbles, apart from the lower current/potential.

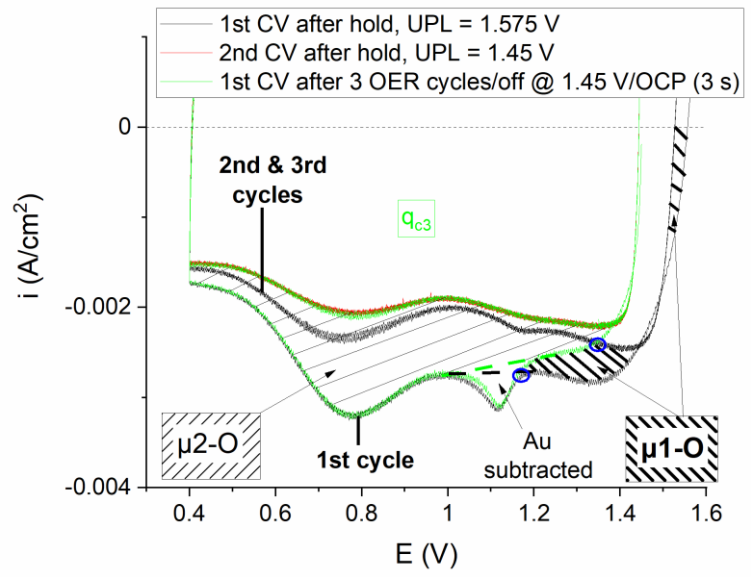

Figure S22: Example of the deconvolution procedure followed to discriminate the charge fractions associated with the reduction/protonation of the high (μ1-O) and low (μ2-O) potential redox active species. The cathodic charge of the first cathodic sweep, measured after potentiodynamic OER/

OCP (green) at the end of the stationary measurements, is used as baseline of the low potential charge (μ2-O species, thin dashed highlighted area). The equation used to calculate the high potential charge (μ1-O species) grown during stationary operation (bold dashed highlighted area) is given below (eq. S1). The common portion of the high potential charge contributions (> 1.45 V) of the sweeps measured after stationary operation without current interruption are not accounted as we are interested in the growth of the fractional charge. The overall cathodic charge of the subsequent CV cycles with upper potential 1.45 V, measured after CA/CV, is the denominator, q(0.4-1.45 V) in Fig. 8 (=q_{c3} in green in Fig. S22), to evaluate the fractional growth of μ1-O and μ2-O species, $q_{\mu\text{-O}}/q$. The dashed lines show the baselines for subtracting the contributions from the reduction of Au oxide, which was always the first step in the data treatment below.

$q_{ci,j}$(x-y) below describes the charge of the cathodic sweep, q_c, i (≤ 3) is the sweep number of the respective CV sequence j (≤ 3) measured after stationary OER operation. x-y is the integration potential limits in V. When j replaced by OER, it refers to the 3 CV cycles measured after OER sweeps, the first cycle of which is the reference for describing μ2-O charge contributions. With these definitions, the charge contributions of the μ1-O species (bold dashed highlighted area in Fig. S22) are given by eq. S1.

$$q_{\mu1\text{-O}} = q_{c1,1}(1.575\text{-}1.2) - q_{c3,1}(1.575\text{-}1.31) - q_{c1,OER}(1.31\text{-}1.2) \quad \text{(S1)}$$

1.2 and 1.31 V are approximate values to describe the two intersecting points of the 1st cathodic sweep after OER sweeping with current interruption with the 1st (at ca. 1.2 V) and 2nd cathodic sweeps measured after CA without current interruption (at ca. 1.31 V), marked with blue circles in Fig. S22. The intersects in the charge deconvolutions per potentiostatic interim varied by ± 30 mV.

The sum of μ1-O and μ2-O charge contributions and that of the μ2-O are given by eqs. S2 and S3.

$$q_{(\mu1\text{-}O+\mu2\text{-}O)} = q_{c1,1}(1.575\text{-}0.4) - q_{c3,1}(1.575\text{-}1.45) - q_{c3,2}(1.45\text{-}0.4) \quad \text{(S2)}$$

$$q_{\mu2\text{-}O} = q_{(\mu1\text{-}O+\mu2\text{-}O)} - q_{\mu1\text{-}O} \quad \text{(S3)}$$

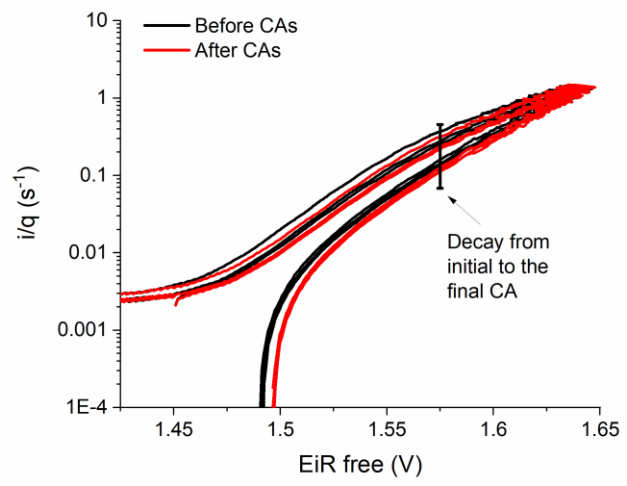

Figure S23: OER sweeps with 2 mV/s before and after the stationary operations with the RDE. The regenerative CVs between and after the stationary interims involved potential excursions down to 0.04 V. The vertical bar displays the activity decay during 8000 s at 1.575 V, RHE. The stationary operation potential was approached with 10 mV/s, resulting in slightly higher initial activity than that of the OER sweeps with 2 mV/s.

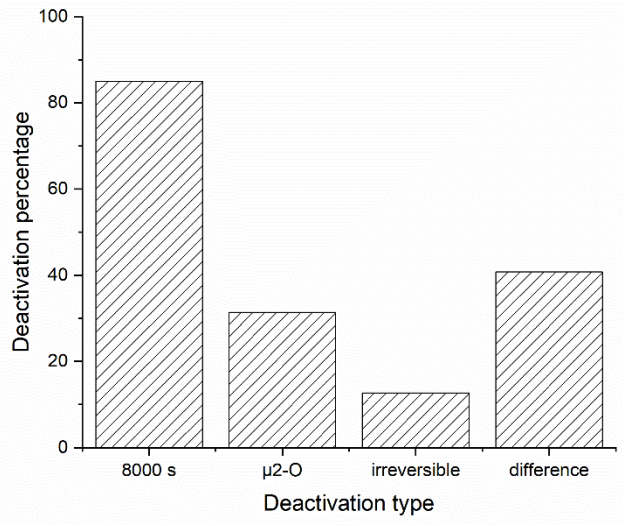

Figure S24: Breakdown of the deactivation percentage over the initial activity in the course of 8000 s at 1.575 V, RHE, into the recoverable portion due to the growth of the μ2-O population (Fig. 8b), an irreversible portion assessed by potentiodynamic OER measurements concomitant to the stationary interims/regenerative CVs (Fig. S23), and the difference from the overall deactivation. The latter deactivation mode, which accounts to roughly 50 % of the overall deactivation, is also recoverable. An additional irreversible degradation due to ECSA loss (base CV charge decrease < 3 % in the course of the stationary interims) is not accounted, as the activities are charge normalized.

7. Stability trends

Calculation of a ML of IrO_2

The volume of 1 ML IrO_2 is $V_{ML} = 2 \cdot d_{Ir\text{-}O} \cdot BET_{SA}$, where BET_{SA} is the BET surface area (≈ 30 m^2/g)[8] and $d_{Ir\text{-}O}$ is the Ir-O bond length (≈ 0.2 nm),[9,10] hence ca. 0.4 nm thickness of 1 ML. The respective mass is $m_{ML} = \rho_{IrO2} \cdot V_{ML}$, where ρ_{IrO2} the density of rutile IrO_2 (=11.7 g/cm^3). Assuming that 1 molecule of IrO_2 is dissolved per Ir atom detected by ICP-MS, the mass of dissolved Ir corresponds to $m_{IrO2\ dissolved} = m_{Ir\ dissolved} \cdot (MW_{IrO2}/MW_{Ir})$.

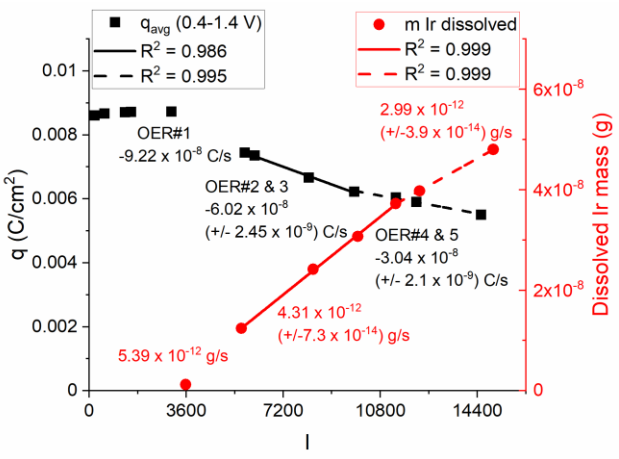

Figure S25: Base CV (0.4-1.4 V, 50 mV/s) charge (black symbols) and accumulated dissolved Ir mass (red symbols) over time of the potentiodynamic regeneration experiment presented in Fig. 9a. The slopes of linear fits mentioned in the figure. The average intrinsic Ir dissolution rate during potentiodynamic OER, which is presented in Fig. 9a with blue symbols, is evaluated by the data herein, by dividing the slopes of dissolved Ir mass and q over the experimental time and further dividing with time under OER conditions, t_{OER}. OER conditions are accounted only when E ≥ 1.45 V, e.g. see Figs. 2a, 3a and S9, neglecting the influence of cathodic dissolution during the regenerative CVs to low potentials, which is one order of magnitude lower (Table 1 in the main).

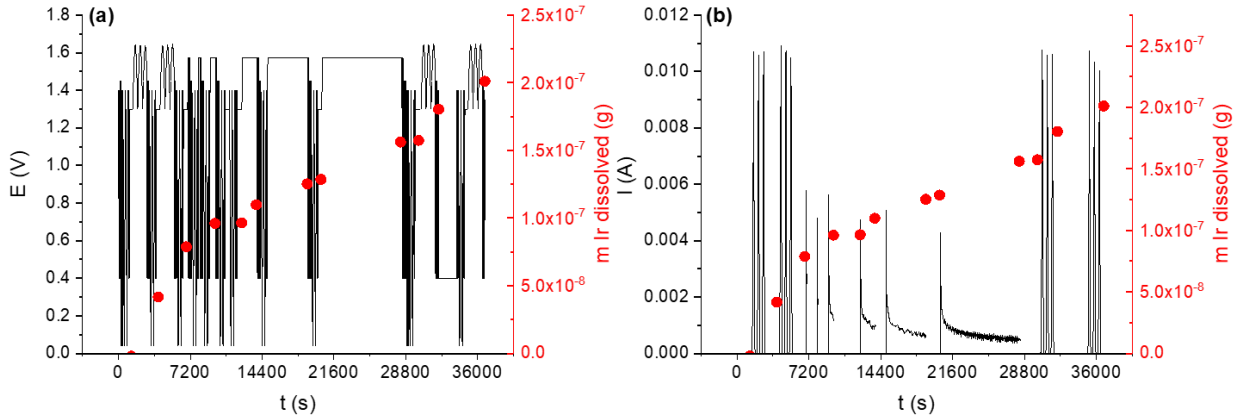

Figure S26: (a) Potential (left y-axis) vs. experimental time during the potentiostatic operation/regeneration experiment shown in Fig. 9b. The accumulated dissolved Ir mass detected by ICP-MS is included (red symbols, right y-axis). **(b)** Respective OER currents when $E \geq 1.45$ V, RHE, assuming 100 % Faradaic efficiency.

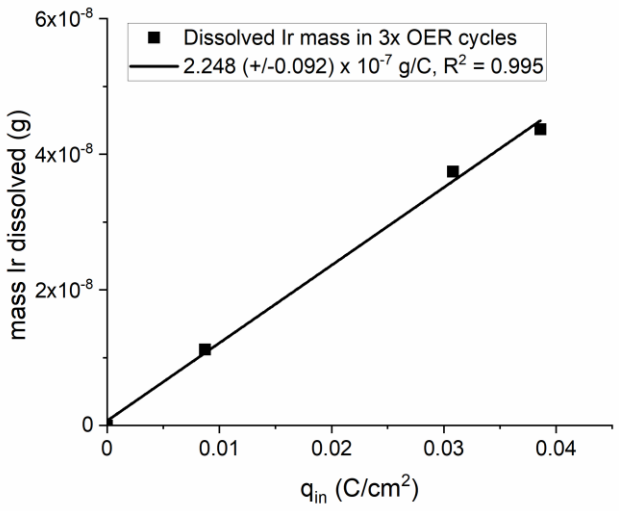

Figure S27: Ir mass dissolved during the first three potentiodynamic OER cycles against the initial CV charge for three different loadings (10-40 µg IrO_x/cm^2 geometric area). The linear regression forced to pass from the origin.

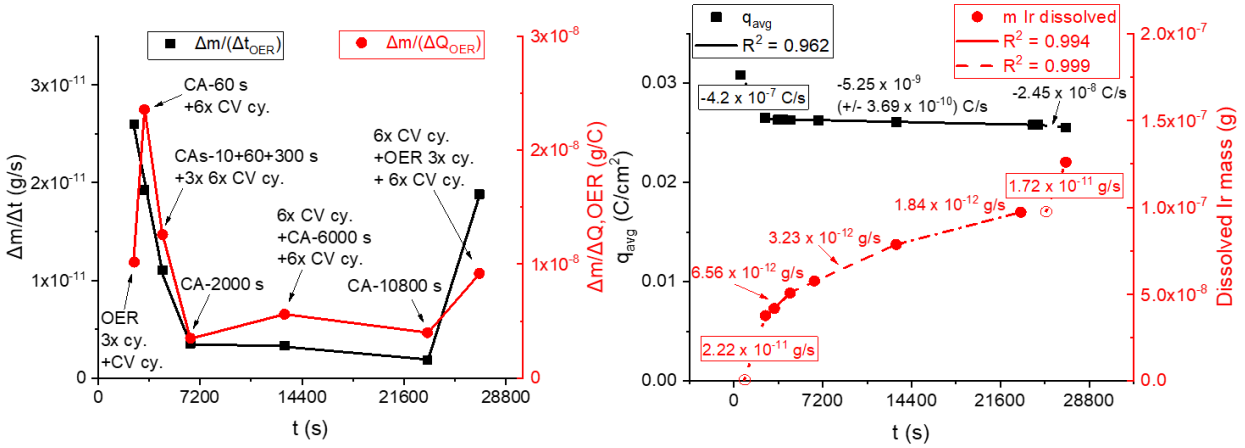

Figure S28: (left) Average Ir dissolution rate (black, left y-axis) and dissolved Ir mass over the OER related charge (red, right y-axis) vs. time of a repeat stationary regeneration experiment as that presented in Fig. 9b. The LPL of the regenerative CVs was kept at 0.4 V. The history before each electrolyte sampling is mentioned in the figure. **(right)** The respective charge (black, left y-axis) and dissolved Ir mass (red, right y-axis) profiles vs. the experimental time. The slopes of the linear fits are mentioned in the figure for comparing with those in Fig. S25.

References

1 C.E. Moore, F. Afsahi, A.P. Young, E.L. Gyenge, *J. Phys. Chem. C*, 2019, **123**, 23361–23373.

2 Parveen, R. Kant, *Electrochim. Acta*, 2013, **111**, 223-233.

3 R. Zhang, N. Dubouis, M.B. Osman, W. Yin, M.T. Sougrati, D.A.D. Corte, D. Giaume, A. Grimaud, *Angew. Chem.*, 2019, **58**, 4571-4575.

4 I. Katsounaros, W.B. Schneider, J.C. Meier, U. Benedikt, P.U. Biedermann, A.A. Auer, K.J.J. Mayrhofer, *Phys. Chem. Chem. Phys.*, 2012, **14**, 7384-7391.

5 M. Seralathan, R.A. Osteryoung, J.G. Osteryoung, *J. Electroanal. Chem.*, 1987, **222**, 69-100.

6 J.H. Christie, P.J. Lingane, *J. Electroanal. Chem.*, 1959, **10**, 176-182.

7 A.J. Bard, L.R. Faulkner, Electrochemical Methods, John Wiley & Sons, 2000, p. 163.

8 V. Pfeifer, T.E. Jones, J.J. Velasco Velez, C. Massue, R. Arrigo, D. Teschner, F. Girgsdies, M. Scherzer, M.T. Greiner, J. Allan, M. Hashagen, G. Weinberg, S. Piccinin, M. Hävecker, A. Knop-Gericke, R. Schlögl, *Surf. Interface Anal*., 2016, **48**, 261-273.

9 H.N. Nong, T. Reier, H.-S. Oh, M. Gliech, P. Paciok, T.H.T. Vu, D. Teschner, M. Heggen, V. Petkov, R. Schlögl, T. Jones, P. Strasser, *Nat. Catal.*, 2018, **1**, 841–851.

10 K. Schweinar, B. Gault, I. Mouton, O. Kasian, *J. Phys. Chem. Lett.*, 2020, **11**, 5008–5014.